

BIOLOGY CONTRIBUTION

**IN VIVO TWO-PHOTON MICROSCOPY STUDY OF SHORT-TERM
EFFECTS OF MICROBEAM IRRADIATION ON NORMAL MOUSE
BRAIN MICROVASCULATURE**

RAPHAËL SERDUC, M.S.,* PASCALE VÉRANT, M.S.,[†] JEAN-CLAUDE VIAL, PH.D.,[†] RÉGINE FARION,*
LINDA ROCAS,* CHANTAL RÉMY, PH.D.,* TAOUFIK FADLALLAH, M.S.,* ELKE BRAUER, M.S.,[‡]
ALBERTO BRAVIN, PH.D.,[‡] JEAN LAISSUE, M.D.,[§] HANS BLATTMANN, PH.D.,^{||}
AND BOUDEWIJN VAN DER SANDEN, PH.D.*

*INSERM, U 594, Functional and Metabolic Neuroimaging, Grenoble, France; Université Joseph Fourier Grenoble, Grenoble, France; [†]CNRS, UMR 5588, Grenoble, France; [‡]European Synchrotron Radiation Facility, Grenoble, France; [§]Institute of Pathology, University of Bern, Bern, Switzerland; ^{||}Paul Scherrer Institute, Villigen, Switzerland

Purpose: The purpose of this study was to assess the early effects of microbeam irradiation on the vascular permeability and volume in the parietal cortex of normal nude mice using two-photon microscopy and immunohistochemistry.

Methods and Materials: The upper part of the left hemisphere of 55 mice was irradiated anteroposteriorly using 18 vertically oriented beams (width 25 μm , interdistance 211 μm ; peak entrance doses: 312 or 1000 Gy). At different times after microbeam exposure, the microvasculature in the cortex was analyzed using intravital two-photon microscopy after intravascular injection of fluorescein isothiocyanate (FITC)-dextran and sulforhodamine B (SRB). Changes of the vascular volume were observed at the FITC wavelength over a maximum depth of 650 μm from the dura. The vascular permeability was detected as extravasations of SRB.

Results: For all times (12 h to 1 month) after microbeam irradiation and for both doses, the FITC-dextran remained in the vessels. No significant change in vascular volume was observed between 12 h and 3 months after irradiation. Diffusion of SRB was observed in microbeam irradiated regions from 12 h until 12 days only after a 1000 Gy exposure.

Conclusion: No radiation damage to the microvasculature was detected in normal brain tissue after a 312 Gy microbeam irradiation. This dose would be more appropriate than 1000 Gy for the treatment of brain tumors using crossfired microbeams. © 2006 Elsevier Inc.

Microbeam radiation therapy, Synchrotron radiation X-rays, Blood–brain barrier, Permeability, Vascular volume, Intravital multiphoton microscopy.

INTRODUCTION

The treatment of high-grade gliomas is based on a multidisciplinary strategy associating surgery, radiotherapy, and chemotherapy. Until now, the treatment of glioblastomas has remained ineffective (1): the median survival time is 3 months without any treatment, and 8 to 12 months after surgery and conventional radiotherapy or radiosurgery (1–3).

The dose for the irradiation of brain tumors is limited by the radiosensitivity of normal adjacent brain tissue (4).

Ionizing radiation may cause delayed complications in normal brain parenchyma, such as radionecrosis, demyelination, glial reaction, vascular damage, and dementia (5–8). Acute important risks of conventional radiotherapy (60 Gy fractionated in 5 weeks) are cerebral edema and intracranial hypertension after a blood–brain barrier (BBB) breakdown (6, 8, 9). The BBB is a functional barrier which ensures the indispensable transport regulation between central nervous system and blood. Many studies reported a significant transient increase in BBB permeability for molecules of inter-

Reprint requests to: Raphaël Serduc, M.S., INSERM U 594, Functional & Metabolic Neuroimaging, Centre Hospitalier Universitaire Pavillon B - BP 217 38043, Grenoble Cedex 09, France. Tel.: (+33) 476765978; Fax: (+33) 476765896; E-mail: rserduc@ujf-grenoble.fr

Presented in part at the second quadrennial meeting of the World Federation of NeuroOncology, Edinburgh, Scotland, May 2005 and at the 22nd annual meeting of the European Society for Magnetic Resonance in Medicine and Biology, Basle, Switzerland, September 2005.

Raphaël Serduc has received a grant from “La ligue contre le

cancer.” This work was further supported by grants from: Ligue contre le cancer (comité de l’Isère); Association pour la recherche sur le cancer; Programme interdisciplinaire CNRS-INSERM-CEA IPA; Région Rhône-Alpes (Appel d’offre thématique cancer); Cancéropôle Lyon Rhône-Alpes.

Acknowledgments—The authors thank Dr. G. Le Duc for critically reading this manuscript, and Benoit Bolliet and Christophe Sibourg for their help in the design and realization of the stereotactic frame.

Received Oct 6, 2005, and in revised form Nov 21, 2005.
Accepted for publication Nov 23, 2005.

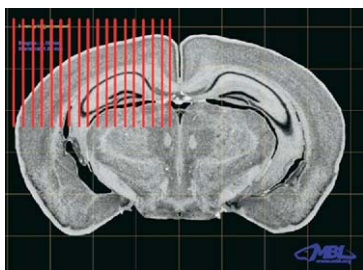


Fig. 1. Anteroposterior microbeam irradiation of the left cerebral hemisphere (coronal section) of a mouse by an array of 18 microplanar-beams of 25 μm width, separated by 211 μm on-center distances.

mediate (1 kD < MW < 30 kD) and high molecular weights (>30 kD) at different times after irradiation (10–12). The increase of the BBB permeability is expected to be important for water, even more than for the different probes described in the literature. This fact may contribute to the pathogenesis of acute neurologic symptoms such as cognitive dysfunction (6, 13).

Therefore, a new radiotherapy treatment that avoids or decreases the risk of a BBB breakdown would be a significant progress. The Microbeam Radiation Therapy (MRT) is an innovative preclinical radiation therapy technique tailored for brain tumors; it may reduce the risk of vascular damage and BBB breakdown. First developed at the National Synchrotron Light Source, Brookhaven National Laboratory (14, 15), it consists of a spatial fractionation of the delivered dose (microplanar beams; Fig. 1). MRT uses high-intensity X-ray beams with negligible divergence generated at a synchrotron radiation source. Microbeam exposures performed on the brain of adult rats (14), suckling rats (16), duck embryos (17), and piglets (18) showed a particular resistance of normal tissues to high X-ray doses. The neuropathologic effects observed on normal rat brains were the loss of neuronal and astrocytic nuclei confined in the path of microbeams (peak regions). Cellular loss was observed in valley regions, i.e., between the microbeams paths, only for skin-entrance absorbed doses ≥ 2500 Gy (14). More recently, Dilmanian *et al.* (19) compared the therapeutic efficiency of MRT and broad-beam radiotherapy on a murine mammary carcinoma implanted in a mouse leg. It appears that a single high-dose irradiation using a unidirectional cross-planar MRT mode (approximately 66 microbeams, 90 μm width each, 300 μm spaced, and 650 Gy skin-entrance dose) has the same tumor ablation rate (75%) as a 45 Gy broad-beam irradiation. Animals irradiated with broad-beam configuration showed epilation, skin desquamation, and severe leg dysfunctions. No side effects were observed after MRT. Laissue *et al.* (15) have studied MRT effects on a 9L-gliosarcoma rat model implanted in brain. By crossfiring microplanar arrays of X-rays, they observed an ablation of the tumor in 22 of 36 rats and minor damages were detected in adjacent brain tissue.

In the last study (15), the integrity of the normal microvasculature in the irradiated microbeam slices and the lack of old

or recent hemorrhage, were checked on histologic sections. The rare fibrinoid necrosis of small vessels irradiated longitudinally, i.e., after irradiation of a >100 micrometer-long blood vessel segment parallel to the microplanes, was deemed to abort reparation of endothelial damage. To explain the sparing effect of microbeam irradiation on normal tissue adjacent to the tumor, it has been hypothesized that nonirradiated endothelial cells between the irradiated zones are able to repair rapidly the microvasculature or the BBB, or both, in the irradiated zones (14, 15).

The hypothesis stated above needs to be tested *in vivo* on animal models before MRT can be used in clinical research protocols. Thus far, little is known about the microbeam irradiation-induced microvascular damage in normal brain tissue at different time delays after irradiation. Further, the repair mechanism of irradiated vessels and the duration of the regeneration process are not well understood. Therefore, the aim of this study was to analyze anatomic and physiologic changes of functional microvessels in normal mouse brain tissue at different time intervals after microbeam radiation exposure. The BBB breakdown and changes in the functional vascular volume induced by radiation were studied by intravital multiphoton microscopy. The presence of viable endothelial cells within vessels in irradiated regions was checked by Platelet Endothelial Cell Adhesion Molecule I (PECAM-I) (20) and type IV collagen (21) immunohistochemistry. Regional blood volume and vascular density modifications were estimated using quantitative immunohistochemistry for type IV collagen protein.

METHODS AND MATERIALS

All experimental procedures were performed in accordance with the French Government guidelines for the care and use of laboratory animals (licenses no. 380321, A 3851610004, and B 3851610003).

Irradiation protocol and instrumentation

Radiation source. The European Synchrotron Radiation Facility (ESRF) located in Grenoble, France consists of an 844-m circumference electron storage ring. The X-ray beam is produced by bunches of 6-GeV electrons circulating at high frequency (355 MHz revolution frequency) in an air-evacuated ring. The maximum current obtained is 200 mA with a lifetime of 60 h. The ID-17 Biomedical Beamline of the ESRF where the X-ray irradiation was performed is devoted to the development of new imaging and radiotherapy protocols by using the synchrotron light.

X-rays used for microbeam radiation therapy were emitted from a wiggler, a linear succession of 21 opposite direction 1.6-Tesla magnets inserted in a straight section of the storage ring. The white beam was filtered by a sequence of beryllium (0.5 mm), carbon (1.5 mm), aluminum (1.5 mm), and copper (1.0 mm) attenuators. The resulting X-ray spectrum extended from approximately 50 to 350 keV with its mean energy around 90 keV. The dose rate after filtering was as high as 86 Gy \cdot s $^{-1}$ \cdot mA $^{-1}$. Only the central cone of the synchrotron beam (0.5 mm high, 4 cm wide) was selected by different set of slits. The quasi-laminar beam was then spatially fractionated into an array of microbeams by using an adjustable multislit collimator (22) positioned approximately 80 cm upstream

from the head of the nude mice. Nude mice were fixed on a high-precision goniometer which was vertically scanned through the microbeam array to deliver the desired dose (Fig. 1). The goniometer was remotely controlled and the translation speed, which determines the delivered dose to the tissues, was kept constant by an automatic feedback system.

Microbeam irradiations. Swiss nude mice (Charles River Laboratories, Inc., Les Oncins, France) approximately 5 weeks old, 14–24 g in weight, were anesthetized with xylazine/ketamine (0.1%/1% in saline buffer, 10 μL per g of body weight) and irradiated in MRT mode. This mouse model will enable analysis of the MRT response of human glioma xenografts in the near future. Mice were placed on a computer-controlled goniometer, and a -7° angle in the longitudinal direction was applied to avoid spinal cord irradiation. The complete immobility of mice during irradiation was checked on-line using three high-resolution video camera systems. The upper part of the left hemisphere was irradiated in the anteroposterior direction by an array of 18 vertically oriented, parallel 25- μm -wide microplanar beams, with on-center 211 μm distances (entrance doses: 312 and 1000 Gy, irradiation field: 4 mm high, 4 mm wide) (Fig. 1). The spatial configuration of the microbeams and the dose were checked by radiochromic films and an ionization chamber.

In vivo multiphoton laser scanning microscopy study

Animal preparation. Microbeam irradiation effects on blood volume and permeability of the cerebral microvasculature were studied *in vivo* at different times (2 h, 12 h, 24 h, 48 h, 4, 7, 12 days, and 1 month) postirradiation. Mice ($n = 55$) were anesthetized with a mixture of xylazine/ketamine (0.1%/1% in saline buffer, 10 μL per g of body weight) and placed on a stereotaxic frame modified to allow anterior-posterior rotation of the animal to optimize laser penetration. A craniotomy of 3 mm in diameter was carried out above the left parietal cortex. The bone was removed, and the exposed cerebral cortex was protected by an agarose gel (23), 1% in 0.9% saline solution. A mixture (100–50 μL) of a 70 kD fluorescein-dextran solution (100 mg \cdot mL $^{-1}$, Sigma-Aldrich, FD-70S) and a 0.58 kD sulforhodamine B (SRB) solution (10 mg \cdot mL $^{-1}$, Lambda Physics) was then injected in the tail vein of the mouse. Core temperature was maintained at approximately 37°C using warm water circulating through a pad, and the head of the mouse was positioned under the 20 \times water-immersion objective.

In vivo two-photon microscopy. Two-photon laser scanning microscopy was performed with a confocal microscope consisting of a Biorad (MRC 1024) scanhead and an Olympus BX50WI microscope. An 800-nm excitation beam from a femtosecond Ti:Sapphire laser (5-W pump; Spectra-Physics, Millennia V) was focused in the sample using a 20 \times water-immersion objective (0.95 numerical aperture, Xlum Plan FI Olympus), and the beam was scanned in the x-y plane to acquire a 512 \times 512 image (0.9 s/image). The z-scan (variation of the observation depth) was realized by vertical motion of the motorized objective. The incident laser intensity was varied by using a polarizer placed before the microscope so that the total average power delivered at the surface ranged from 20 to 200 mW. Typically, an energy of 10 $^{-8}$ J is deposited on a surface of approximately 1 μm^2 [$= \pi(0.6 \mu\text{m})^2$] in the focal region. The exciting light is attenuated by scattering/absorption of ballistic photons, and the emitted light is decreased by absorption of fluorescence photons by cerebral tissue (24). To counter this, the intensity of the laser was manually increased as the depth increased to such a level that the fluorescence from a few pixels saturated the detection system. Fluorescence was collected

with two added external photomultiplier tubes. Filters in front of these tubes separated the red fluorescence (rhodamine emission) from the green one (fluorescein emission) so that two dyes could be simultaneously observed. Image acquisition and reconstruction were performed using the Biorad exploitation system. Planar scans of the fluorescent intensity were acquired at successive depths in the cortex. The z-step between scans ranged from 1 to 5 microns; acquisition of a stack took 1–2 min. Images were analyzed using Image J (ImageJ, v.1.33 Public Domain Software, available on <http://rsb.info.nih.gov/ij/>, 2005) and home-made software.

Immunohistologic study

Histologic analyses were performed on two groups of mice irradiated as described previously. The first group ($n = 87$) was used to assess the short-term effects of microbeam irradiation on brain cells at different times after exposure (2, 12, 24 h, 2, 4, 7, 12 days). Hematoxylin–eosin (HE) staining was performed on all mice, whereas type IV collagen and PECAM-I immunohistochemistry was only achieved on few animals. The second group of irradiated mice was used for brain vascular parameters quantification at 12 h, 12 days, 1 and 3 months after microbeam exposure ($n = 4$ –5 per delay and dose). HE, type IV collagen and PECAM-I immunohistochemistry was performed.

Section preparation

Mice were killed by neck dislocation. The brain was excised and frozen in isopentane at -50°C . Horizontal frozen sections (10 μm thick) were obtained with a cryotome at -18°C and stained with HE.

Immunofluorescence assays

Multiple immunofluorescence stainings were performed on adjacent sections to study the capillary network. Nonspecific labeling was prevented by preincubating sections with 5% bovine serum albumin in phosphate-buffered saline, 30 min at room temperature. Next, the sections were incubated for 16 h at 4°C with the primary antibodies, rat polyclonal against PECAM-I (20) (1/200, TEBU bio) and a goat polyclonal anti-type IV collagen (1/1000, F-5202 VF83, UNLD) as described previously (21). Sections were washed 4 times with phosphate-buffered saline, then exposed to the secondary antibodies for 4 h at room temperature. Fluorescein isothiocyanate (FITC)-conjugated donkey anti-goat F(ab') $_2$ (1/100, Jackson ImmunoResearch Laboratories, Inc.), Tetramethylrhodamine B isothiocyanate (TRITC)-conjugated donkey anti-rat F(ab') $_2$ (1/100, Jackson ImmunoResearch, Inc.), and nuclei were counterstained by 4,6'-diamidino-2-phenylindole (DAPI) (1 $\mu\text{g} \cdot$ mL $^{-1}$ in mounting medium) (25). The immunohistologic staining of type IV collagen, localized in the basal membrane of blood vessels, allowed the detection of all blood vessels and capillaries. Staining of PECAM-I indicated the presence of endothelial cells and intercellular junctions. The sections were examined with a Nikon Eclipse E600 microscope (Nikon, Champigny sur Marne, France) equipped for epifluorescence with 10 \times and 20 \times air-immersion objectives to check the presence of vessels and of viable endothelial cells after irradiation.

Quantitative image analysis

Quantitative image analyses were performed 12 h, 12 days, 1 month, and 3 months after microbeam exposure. The number of mice per time delay was 4–5. The number of coronal brain tissue sections per mouse varied between 14 and 20 with a mean inter-

distance of 60 μm . Total vessels and endothelial cells were stained by immunohistochemistry of type IV collagen and PECAM-I as described previously.

Images were acquired using a confocal microscope Olympus Fluoview BX50 based on two lasers (Arg 488 nm, HeNe 543 nm) and two photomultipliers for specific light detection. For all brain slices, a field of view of $707 \times 707 \mu\text{m}$ was acquired in the parietal cortex of the irradiated hemisphere and in the ipsilateral hemisphere at the same location. All field of views were sampled at equal distances (500 μm) from the brain midline, and they nearly covered the whole parietal cortex of the mice, which is approximately 800 μm thick. This was approximately the location of the cranial window in the two photon microscopic studies. The volume of interest in the irradiated and ipsilateral parietal cortex ranged from 0.5 mm^3 (14 slices) to 0.67 mm^3 (20 slices) including the slice thickness.

Next, a homemade macro (Kontron KS 400, Zeiss; Carl Zeiss AG, Oberkochen, Germany) was used for image processing and analysis of morphometric parameters per time delay after microbeam exposure.

Image processing

After an adaptive gray value segmentation of the original gray value images (8 bits), we eliminated structures with areas smaller than 15 pixels, which were related to nonspecific staining. Microvessels with a noncontinuous collagen IV staining were closed, and the vessel lumina were filled. Finally, the original gray value image and the processed binary image were overlaid, and we checked manually if the areas of the microvascular structures after image processing were not larger than in the original gray value image.

Image analysis

The mean vessel density (n/mm^2) and the vascular volume per tissue volume of interest (%) were estimated for each mouse. The vessel density for each mouse was reported as the mean of vascular density of all sections. The vascular volume (V_v) for each mouse was estimated according to the stereological algorithm of Adair *et al.* (26).

$V_v = [\pi/4 \cdot (\text{Mean diameter})^2 \cdot L_v]$, where L_v is the vascular length density per volume of reference. The mean vessel diameter for each mouse was calculated for all sections. L_v was estimated according to the formula $L_v = \Sigma a/b / \Sigma A_i$ (26) where microvessels were considered as perfect cylinders. $\Sigma a/b$ is the sum of the ratio of the major axis (a) to the minor axis (b) of all vessels per mouse; ΣA_i is the sum of all field of views per mouse. The vascular volume per tissue volume of interest was obtained by dividing the vascular volume estimated for each mouse by the volume of interest. The values reported in tables are the average results over all 4–5 mice per group. Differences in morphometric parameters of the microvasculature in the irradiated and nonirradiated hemisphere were analyzed by a paired *t* test using GraphPad Prism version 4.00 for Windows (GraphPad Software, San Diego CA).

RESULTS

Postirradiation animal behavior

After irradiation with either of the two doses, all mice were alive during the whole observation period of 3 months. Neurologic tests were not performed, but a follow-up of the body weight during 3 months on groups of mice irradiated

at 312 Gy ($n = 6$) and 1000 Gy ($n = 7$) did not reveal any differences compared with the weight curves reported by the animal supplier. After application of a dose of 312 Gy, the behavior of the mice seemed normal, with changes in neither motor functions nor social behavior. On the other hand, animals irradiated with a higher dose (1000 Gy) showed signs of hyperactivity that disappeared 4 h after irradiation. A weak radiodermatitis was observed in the path of microbeams during approximately 12 days after microbeam exposure with an entrance dose of 1000 Gy. The skin recovered and appeared normal 1 month after irradiation. Some mice have been kept alive for 6 to 24 months after irradiation and currently present only a slight atrophy of eye and signs of cataract.

Postirradiation histologic analysis

Hematoxylin-eosin-stained sections revealed cellular damage induced by microbeams. Twelve hours after microbeam irradiation (312 and 1000 Gy), dark striae were observed at low magnification (Fig. 2), especially in high nuclear density regions such as the granular layer of the cerebellum. These striae, which were separated by approximately 200 μm , correspond to the irradiated microslices. At high magnification, nuclear condensation—nuclear pyknosis—could be observed, i.e., an indication of cell death (Figs. 2a and 2b, black arrows). At longer postirradiation delays, the number of glial and neuronal cells decreased quickly in the microbeam stripes until an almost complete disappearance of cellular bodies and nuclei 7 days after

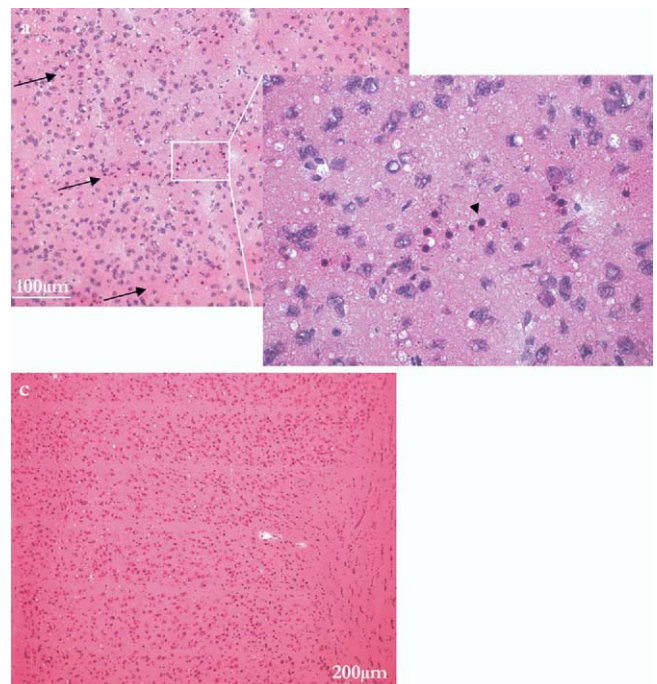


Fig. 2. Coronal section of a left parietal cortex mouse brain 24 h (a and b) and 3 months (c) after microbeam irradiation with 25- μm -wide microbeams, 211- μm center-to-center spacing, skin entrance dose of 1000 Gy (frozen section, hematoxylin and eosin). Arrows: microbeam paths; arrowhead: pycnotic nuclei.

radiation exposure. The microbeam stripes then appeared on HE-stained sections as pale striae (Fig. 2c). These striae were still observed 3 months after microbeam irradiation. Repopulation of irradiated slices by cells was not observed during this period. After application of either of the incident radiation doses, hemorrhages or tissue necrosis were never observed in the irradiated hemisphere. The cellular effects observed after 312 Gy or 1000 Gy exposure evolved with great morphologic and temporal similarity.

In vivo multiphoton imaging of BBB breakdown and functional vascular density

Multiphoton excitation provides images of brain vasculature as far as 650 μm below the dura. This value represents approximately 75% of the mouse brain cortical layers. At a depth of 50–100 μm , the penetrating vessels divided into numerous branches and in capillaries which were not seen at the surface. To estimate cerebral blood volume and permeability of the BBB modifications after microbeam irradiation, fluorescent molecules were injected intravenously, one of large size, which remain intravascular despite the radiation treatment (fluorescein-dextran, 70 kD), and a smaller probe (SRB, 0.58 kD) that diffuses across vascular endothelium when the BBB leaks. In preliminary studies on normal unirradiated control animals ($n = 6$), diffusion of both fluorescent probes was tested by intravital multiphoton microscopy. The observation of the parietal cortex from the pial vessels to capillaries situated at 650 μm depth did not reveal any extravasation of FITC-dextran or any enhancement of SRB diffusion into the extravascular compartment (data not shown).

At any time after irradiation with either 312 Gy or 1000 Gy, FITC-dextran remained intravascular. Capillaries situated within or between the microbeam paths were perfused, and there was no obvious difference in capillary density between irradiated microslices and tissue regions situated between the irradiated microslices (Figs. 3a, 3c, and 3e). However, when the microbeam hit a plunging vessel longitudinally along 50 to 100 μm , a halo of FITC-dextran 70 kD could be observed around the vessel situated in the axis of the microplanar stripes (data not shown).

All mice exposed to 312 Gy skin entrance dose never showed diffusion of SRB in the extravascular compartment (Fig. 3b). The capillary density was constant, and the vascular network remained completely perfused. In mouse brains exposed to a 1000 Gy skin entrance dose, a diffusion of SRB was detected in the microbeam stripes. All results are summarized in Table 1, where localized diffusion of SRB in the microbeam stripes per number of mice is reported. Twelve hours after microbeam exposure, a homogenous diffuse signal of SRB was observed in the extravascular compartment but only in the microbeam paths (Fig. 3d). Twenty-four to 48 h postirradiation, only dotted signals of SRB (4 to 6 μm in diameter) could be detected in the microbeam paths (Fig. 3f). Four to 12 days later, these dotted signals became smaller, and they decreased in density. Three mice studied 1 month after irradiation did not show the presence of extravascular SRB (data not shown).

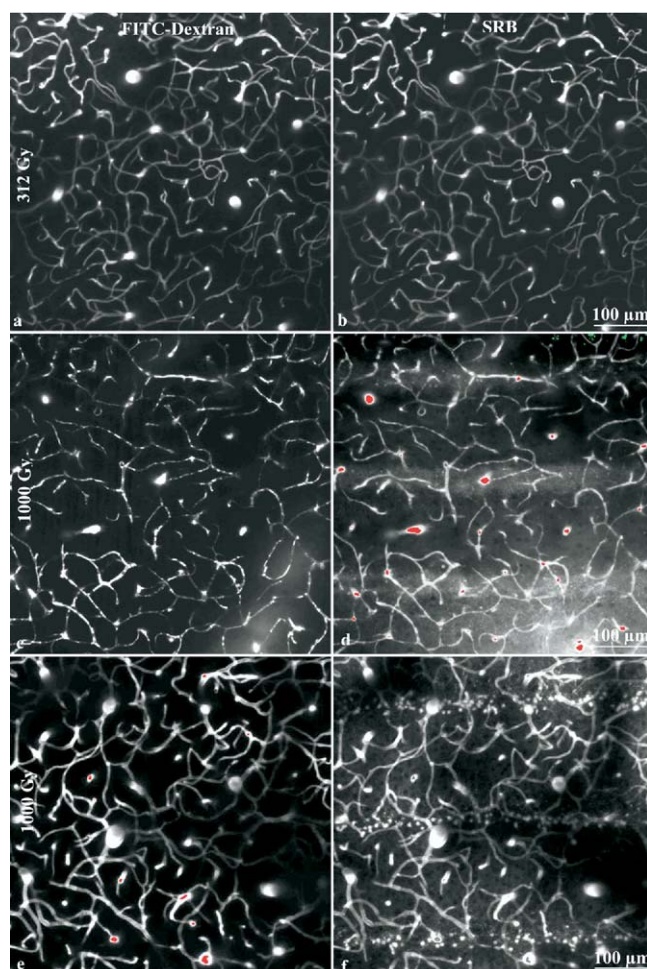


Fig. 3. Z-projection of images acquired *in vivo* from 200 to 300 μm (a and b), 50 to 100 μm (c and d), and 150 to 250 μm (e and f) below the dura (2- μm steps) in the left parietal cortex of a nude mouse 12 h after 312 Gy (a and b), 12 h after 1000 Gy (c and d), and 48 h after 1000 Gy entrance dose exposure (e and f). The mouse was injected intravenously with 100 μL of 100 $\text{mg} \cdot \text{mL}^{-1}$ fluorescein isothiocyanate-dextran solution and 50 μL of a 5 $\text{mg} \cdot \text{mL}^{-1}$ sulforhodamine B solution approximately 2 min before microscopy. Filters in front of two photomultiplier tubes separate the green fluorescence (from fluorescein isothiocyanate-dextran emission, images a, c, and e) from the red one (from sulforhodamine B emission, images b, d, and f).

Immunohistochemistry and blood volume estimation

Microbeam paths could not be identified on the basis of type IV collagen and PECAM-I immunostaining but were detectable with DAPI nuclear labeling (25). Endothelial cells were present in the irradiated tissue microslices after both radiation doses (312 Gy or 1000 Gy) and at any time after radiation exposure (12 h to 3 months). Each blood vessel and capillary detected in the irradiated microslices or in the tissues situated between those microslices revealed double staining for the type IV collagen and PECAM-I proteins (Fig. 4).

Quantitative analysis of blood volume and vascular density confirms the qualitative observations of type IV collagen stained sections. The results are summarized in Tables

Table 1. Diffusion of Sulforhodamine B at different times after microbeam exposure

Doses	Observation delays							
	2 h	12 h	24 h	48 h	4 days	7 days	12 days	30 days
312 Gy	0/3	0/3	0/2	0/3	0/3	0/3	0/3	—
1000 Gy	0/4	3/3	4/4	5/5	6/6	4/4	6/6	0/3

The local diffusion of Sulforhodamine B in irradiated peak regions per fraction of animals studied is shown.

2 and 3. No significant difference in morphometric parameters of the capillary network was found during the first 3 months after microbeam exposure whatever the deposited dose. Cerebral blood volume ranged from $2.41 \pm 0.35\%$ to $3.47 \pm 0.33\%$ in the contralateral hemisphere and ranged from $2.51 \pm 0.61\%$ to $3.64 \pm 0.35\%$ in the irradiated cortex (312 Gy and 1000 Gy; Table 2). For both doses, the vessel density did not change significantly during 3 months after microbeam irradiation (Table 3) and no apparent difference was found between the irradiated and contralateral hemisphere, whatever the dose and time after radiation exposure.

DISCUSSION

We have investigated the short-term effects of microbeam irradiation on the normal mouse brain at high doses of synchrotron generated X-rays with high dose rates ($86 \text{ Gy} \cdot \text{s}^{-1} \cdot \text{mA}^{-1}$) and an energy spectrum ranging from 50 to 350 keV. The BBB permeability to large and small

fluorescent compounds has been analyzed *in vivo*, as well as effects of microbeam radiation exposure on morphometric parameters of the brain vascular network (vessel density, regional cerebral blood volume). Our findings suggest that a single unidirectional irradiation of mouse brain cortex by eighteen $25\text{-}\mu\text{m}$ -wide microbeams with $211\text{-}\mu\text{m}$ on-center distances and using skin entrance doses of 312 or 1000 Gy, does not induce blood volume change, hemorrhage, inflammatory response, or tissue necrosis. Only a transient increase of BBB permeability to small molecules has been observed after a 1000 Gy microbeam exposure.

Multiphoton microscopy is a very promising tool to investigate physiologic processes in living animals with a subcellular resolution (27–29). This recent technique has already been applied to study several animal tissues, e.g., kidney (30), brain (23, 31), and tumors (32). In our study, we have been able to observe brain microvasculature to a tissue depth of $650 \mu\text{m}$ and to provide evidence that capillaries situated in the irradiated microslices were not affected and remained perfused, for both skin entrance doses and at any time after irradiation. No obvious modification of cerebral blood volume could be detected in irradiated hemisphere. However, if qualitative observations of biologic systems are feasible with multiphoton microscopy, quantitative measurements are less straightforward owing to the influence of several parameters on the analysis of multiphoton data (24, 33). Work is in progress to obtain quantitative cerebral blood volume measurement from multiphoton microscopy (34). Meanwhile quantitative analysis of cerebral blood volume was performed using stereological methods.

Immunohistologic study of frozen brain slices revealed that capillaries observed in the microbeam slices (peak regions) as well as the capillaries situated between the microbeam slices (valley regions), expressed type IV collagen and PECAM-I proteins. From 12 h to 3 months after microbeam exposure, the vascular volume and the capillary density were not significantly different between the irradiated and the contralateral hemisphere, corroborating the multiphoton microscopy observations. Conversely, it has been shown that fractionated stereotactic radiotherapy of brain tumors induced important blood volume changes in normal adjacent tissue (35). Nowadays, there seems to be consensus that microvasculature sparing is the major advantage of MRT vs. conventional radiotherapy, even if the repair mechanisms are not yet fully understood. A recent study showed that a 150 Gy skin entrance dose irradiation

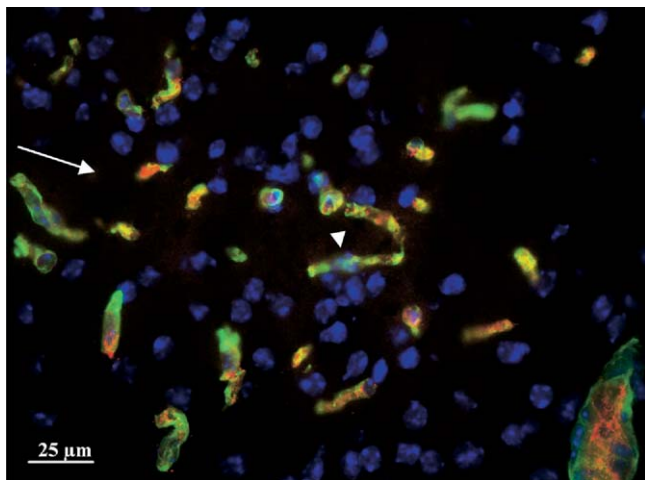


Fig. 4. Type IV collagen (fluorescein isothiocyanate labeling) and platelet endothelial cell adhesion molecule I (Tetramethylrhodamine B isothiocyanate [TRITC] labeling) immunostaining. Horizontal section of a left parietal cortex mouse brain 3 months after microbeam irradiation with $25\text{-}\mu\text{m}$ -wide microbeams, $211\text{-}\mu\text{m}$ center-to-center spacing, skin entrance dose of 1000 Gy. The arrow shows a microbeam stripe in the motor cortex. An important loss of cell nuclei (4,6'-diamidino-2-phenylindole [DAPI]) has been observed in the microbeam path but immunoreactivity for endothelial cells (platelet endothelial cell adhesion molecule I positive expression, arrowhead) remains detectable in the irradiated microslices ($10\text{-}\mu\text{m}$ -thick frozen section).

Table 2. Cerebral blood volume evolution after microbeam exposure

Time after MRT	312 Gy	Contralateral	1000 Gy	Contralateral
12 h	2.51 ± 0.61	2.41 ± 0.35	2.54 ± 0.52	2.68 ± 0.39
12 days	3.28 ± 0.44	3.35 ± 0.41	3.35 ± 0.30	3.25 ± 0.20
1 month	3.34 ± 0.67	3.17 ± 0.52	3.64 ± 0.35	3.47 ± 0.33
3 months	3.04 ± 0.47	3.06 ± 0.54	3.19 ± 0.87	3.26 ± 0.52

Estimations of the cortical blood volume (%) 12 h, 12 days, 1 and 3 months after microbeam irradiation (312 and 1000 Gy) in the nonirradiated (contralateral) and irradiated parietal cortex of nude mice. Mean values with their standard deviations are reported. Differences between the ipsilateral and contralateral hemispheres were not significant: two-tailed *p* values (paired *t* test) >> 0.05.

(27 μm microplanar width, 200 μm on-center spacing) is well tolerated by rat carotid artery and was considered as an insufficient dose to significantly suppress the neointimal hyperplasia observed after balloon angioplasty (36).

Several hypotheses have been formulated to explain this surprising radio-resistance of normal brain capillaries after microbeam exposure. The most plausible one was the migration or division of minimally irradiated surviving endothelial cells adjacent to microbeam regions (14). In 1981, Reidy and Schwartz showed that aorta reendothelialization of small areas took place rapidly after injury (37). A 25-μm wound was caused on rat aorta with a nylon microfilament. A longitudinal wound which removed 3 to 5 endothelial cells could be repaired by cell mitosis within 72 h, and this increased cell density remained over the site of injury for at least 4 weeks. When the wound was performed perpendicularly to the endothelial cell alignment (circumferential injury), the authors demonstrated that the reparation of the lesion occurred within 8 h after injury, without cell division. It has been suggested that cytoskeletal and cytoplasmic extensions of endothelial cells might cover a small defect rapidly. It is possible that the same phenomenon takes place after microbeam irradiation of the brain vasculature. The random orientation of brain capillaries decreases the probability of their longitudinal irradiation. As we have noted in our study, large vessels and those oriented parallel to the longitudinal axis of microbeam planes seem to be more vulnerable to microbeam irradiation. Beams used in this work were approximately 25 μm wide and might have allowed rapid vascular reparation such as described by Reidy and Schwartz (37). Such a repair mechanism would

depend less on the skin entrance dose than on the microplanar width and spacing, because we observed no difference between the brains exposed to 312 Gy and 1000 Gy. Other experiments should be performed to find the maximum microbeam width and spacing that would still permit the rapid endothelium regeneration at different dose levels.

The permeability of the BBB to SRB increased between 12 h to 12 days after microplanar irradiation and vanished between 12 and 30 days, but only for a skin entrance dose of 1000 Gy. It has been reported that broad-beam irradiation of the whole body and brain induces BBB permeability modifications which were strongly dependent on the probes (10–12, 38). Immunoreactivity for serum albumin after a single seamless irradiation of a rat hemisphere (20 or 40 Gy conventional X-rays) showed albumin diffusion through the BBB between 1 day to 14 days postirradiation (12). The detection increased on Day 3 and gradually decreased, until albumin became undetectable on Day 30. The time course of BBB recovery kinetic described is comparable to the results obtained in our study. However, after microbeam irradiation, the leakage of the BBB occurred for a smaller probe (SRB 0.58 kD) and only after a 1000 Gy skin entrance dose. Diffusion of the FITC-dextran (70 kD, molecular size similar to that of albumin) was never observed after a 1000 Gy or 312 Gy exposure. Interestingly, Yuan *et al.* (11) have shown on normal rat brain that radiation-induced permeability of the BBB was principally the result of an increase of paracellular transport secondary to tight junction alterations. They demonstrated that a 20 Gy broad beam (6-MV X-rays) is sufficient to increase significantly diffusion of FITC-dextran (4.4 to 70 kD) through brain vessels. The lack

Table 3. Cerebral vascular density evolution after microbeam exposure

Time after MRT	312 Gy	Contralateral	1000 Gy	Contralateral
12 h	415 ± 72	405 ± 84	396 ± 42	401 ± 47
12 days	430 ± 29	433 ± 35	456 ± 71	445 ± 41
1 month	470 ± 73	446 ± 34	412 ± 42	381 ± 26
3 months	444 ± 35	435 ± 25	431 ± 37	427 ± 31

Estimations of the cortical capillary density (number of capillaries per mm²) 12 h, 12 days, 1 and 3 months after microbeam irradiation (312 and 1000 Gy) in the nonirradiated (contralateral) and irradiated parietal cortex of nude mice. Mean values with their standard deviations are reported. Differences between the ipsilateral and contralateral hemispheres were not significant: two-tailed *p* values (paired *t* test) >> 0.05.

of diffusion of large molecules through the BBB after microbeam exposure reveals a new advantage of this irradiation mode spatially fractionated at a microscopic scale. In this case, radiation doses can be considerably increased without provoking important BBB permeability modifications in normal tissues. These results are concordant with the recent study carried out by Dilmanian *et al.* (39) who showed that the BBB breakdown for albumin-FITC took place only in 9L gliosarcoma tumoral vessels—which were not permeable before MRT—and not in capillaries in normal brain tissue after microbeam irradiation (entrance dose 800 Gy, microplanar width 27 μm , microplanar spacing 200 μm) (39).

The dose-dependent response of BBB for small molecules to microbeam irradiation could be explained by considering the physical properties of the beam. It appears that the normal tissue-sparing effect of MRT depends considerably on irradiation parameters such as microplanar beam width and spacing (14). Correct microdosimetry and Monte Carlo simulations are essential for establishing correlation with biologic effect (40). Several groups are working on new irradiation protocols, microdosimetry, and simulation methods (41–46). It is important to note that the dose in the valley regions is not negligible. Radiation damage and cellular stress may extend to a larger area because of the Gaussian shape of each microbeam. Ideally, a perfect microbeam is close to a square with round edges, but in reality, because of the imperfections of the multislit collimator and the divergence of the incoming beam, the microbeam shape becomes more like a Gaussian. Furthermore, X-ray scattering, photoelectrons, and Compton electrons contribute to the dose deposited in the valleys. This dose depends on different criteria such as the absorbed doses, photon energy spectrum, microbeam width, distance between microbeams, number of microbeams, total irradiated volume, and many other factors. In our study, the skin entrance dose was the only parameter that has been modified. However, when the peak dose increases from 312 to 1000 Gy, the entrance dose in the valley estimated by Brauer *et al.* on Matlab home-made software may vary from 5.8 to 18.9 Gy (personal communication, E. Brauer, European Synchrotron Radiation facility Grenoble, France, 2005). A seamless dose of 18.9 Gy delivered to a relatively large brain volume is thought to likely approach or exceed the threshold tolerance dose for normal brain tissue. This might explain the difference observed for SRB leakage through the BBB after 1000 Gy vs. 312 Gy irradiations. The 18.9 Gy presumably absorbed by endothelial cells in the valley region in the vicinity of the irradiated microslices may be too high to allow a rapid recov-

ery of the microvasculature targeted by the whole microbeam array, in contrast to the 5.8 Gy valley dose generated by a 312 Gy exposure. The valley dose appears to be a very important factor in microbeam irradiation.

Multiphoton *in vivo* microscopy has shown that SRB signals in the extravascular compartment after a 1000 Gy exposure change from a diffuse staining 12 h after irradiation (Fig. 3d) to a more dotted staining 12 h later (diameter 4–6 μm ; Fig. 3f). The number of SRB dotted signals decreased in time until they became undetectable after 1 month. These data have to be compared with histologic findings. Cell death induced by ionizing radiation was detectable as soon as 2 h after exposure. One day postirradiation, microbeam stripes were clearly detectable. Nuclei situated in the microbeam stripes showed a strong chromatin condensation suggesting the presence of nuclear pyknosis and incipient cell death. From 4 days to any time after irradiation, the numbers of cells in the microbeam stripes decreased rapidly until only a few intact cells remained in the microplanar stripes after entrance doses of 312 Gy or 1000 Gy. The number of nuclei decreased at the same rate for both doses. The cytotoxic effects of 312 Gy and 1000 Gy in the microbeam stripes may be equivalent. Regarding multiphoton microscopic results, we thus hypothesize that, after a 1000 Gy skin entrance dose microbeam irradiation, SRB leaks through the BBB into the extravascular compartment of the microbeam stripes. Twenty-four hours after exposure, SRB may be endocytosed by microglial cells or may diffuse into radiation-damaged cells situated in the microbeam planes. The cell membrane may be more permeable and therefore facilitates the diffusion of SRB into the cells and the fixation of SRB on cytoplasmic and nuclear proteins. SRB diffusion has never been detected in our intravital microscopy study after a 312 Gy skin entrance dose. Despite the presence of cellular damages similar to those observed after a 1000 Gy exposure, SRB dotted signals were never detected after a 312 Gy irradiation, because of the integrity of the BBB.

In conclusion, up to 3 months after microbeam radiation exposure no changes in blood volume and vascular density were detected in the irradiated microbeam slices of normal brain tissue after a 312 Gy and 1000 Gy exposure. However, the high dose induced BBB leakage for small molecules between 12 h and 12 days after microbeam exposure. The apparent integrity of the BBB after exposure to 312 Gy may indicate that this dose is more adapted to spare normal vascular tissue and to limit cerebral edema. Therefore, this dose may be more appropriate, in terms of normal tissue tolerance, for the treatment of brain tumors using crossfired microbeams.

REFERENCES

1. Black P. Management of malignant glioma: Role of surgery in relation to multimodality therapy. *J Neurovirol* 1998;4:227–236.
2. Salzman M. Survival in glioblastoma: Historical perspective. *Neurosurgery* 1980;7:435–439.
3. de Crevoisier R, Pierga JY, Dendale R, *et al.* [Radiotherapy of glioblastoma]. *Cancer Radiother* 1997;1:194–207.
4. Belka C, Budach W, Kortmann RD, *et al.* Radiation induced CNS toxicity—molecular and cellular mechanisms. *Br J Cancer* 2001;85:1233–1239.

5. Ng W-K. Radiation associated changes in tissues and tumors. *Current Diagnostic Pathol* 2003;9:124–136.
6. Bertrand C, Liang M. Radiation-associated neurotoxicity. *Hospital Physician* 1999;35:54–58.
7. Lamproglou I, Chen QM, Boisserie G, *et al.* Radiation-induced cognitive dysfunction: An experimental model in the old rat. *Int J Radiat Oncol Biol Phys* 1995;31:65–70.
8. Plowman PN. Stereotactic radiosurgery. VIII. The classification of postradiation reactions. *Br J Neurosurg* 1999;13:256–264.
9. Reinhold HS, Keyeux A, Dunjic A, *et al.* The influence of radiation on blood vessels and circulation. XII. Discussion and conclusions. *Curr Top Radiat Res Q* 1974;10:185–198.
10. Diserbo M, Agin A, Lamproglou L, *et al.* Blood-brain barrier permeability after gamma whole-body irradiation: An in vivo microdialysis study. *Can J Physiol Pharmacol* 2002;80:670–678.
11. Yuan H, Gaber MW, McColgan T, *et al.* Radiation-induced permeability and leukocyte adhesion in the rat blood-brain barrier: Modulation with anti-ICAM-1 antibodies. *Brain Res* 2003;969:59–69.
12. Nakata H, Yoshimine T, Murasawa A, *et al.* Early blood-brain barrier disruption after high-dose single-fraction irradiation in rats. *Acta Neurochir (Wien)* 1995;136:82–86; discussion 86–87.
13. Werner-Wasik M, Rudoler S, Preston PE, *et al.* Immediate side effects of stereotactic radiotherapy and radiosurgery. *Int J Radiat Oncol Biol Phys* 1999;43:299–304.
14. Slatkin DN, Spanne P, Dilmanian FA, *et al.* Subacute neuropathological effects of microplanar beams of x-rays from a synchrotron wiggler. *Proc Natl Acad Sci USA* 1995;92:8783–8787.
15. Laissue JA, Geiser G, Spanne PO, *et al.* Neuropathology of ablation of rat gliosarcomas and contiguous brain tissues using a microplanar beam of synchrotron-wiggler-generated X rays. *Int J Cancer* 1998;78:654–660.
16. Laissue JA, Lyubimova N, Wagner HP, *et al.* Microbeam radiation therapy. *Proc SPIE* 1999;3770:38–45.
17. Dilmanian FA, Morris GM, Le Duc G, *et al.* Response of avian embryonic brain to spatially segmented x-ray microbeams. *Cell Mol Biol (Noisy-le-grand)* 2001;47:485–493.
18. Laissue JA, Blattmann H, Michiel D, *et al.* The weanling piglet cerebellum: A surrogate for tolerance to MRT (microbeam radiation therapy) in pediatric neuro-oncology. *Proc SPIE* 2001;4508:65–73.
19. Dilmanian FA, Morris GM, Zhong N, *et al.* Murine EMT-6 carcinoma: High therapeutic efficacy of microbeam radiation therapy. *Radiat Res* 2003;159:632–641.
20. Newman PJ. The biology of PECAM-1. *J Clin Invest* 1997;100:S25–29.
21. Rijken PF, Bernsen HJ, van der Kogel AJ. Application of an image analysis system to the quantitation of tumor perfusion and vascularity in human glioma xenografts. *Microvasc Res* 1995;50:141–153.
22. Archer D. Collimator for producing an array of microbeams. U.S. Patent; 1998.
23. Kleinfeld D, Denk W. Two-photon imaging of cortical microcirculation. In: Yuste R, Lanni F, Konnerth A, editors. *Imaging neurons: A laboratory manual*. Cold Spring Harbor, NY: Cold Spring Harbor Press; 1999. p. 23.15–23.21.
24. Beaurepaire E, Oheim M, Mertz J. Ultra-deep two-photon fluorescence excitation in turbid media. *Optics Commun* 2001;188:25–29.
25. Kapuscinski J. DAPI: A DNA-specific fluorescent probe. *Bio-tech Histochem* 1995;70:220–233.
26. Adair TH, Wells ML, Hang J, *et al.* A stereological method for estimating length density of the arterial vascular system. *Am J Physiol* 1994;266:H1434–1438.
27. Denk W, Strickler JH, Webb WW. Two-photon laser scanning fluorescence microscopy. *Science* 1990;248:73–76.
28. Xu C, Zipfel W, Shear JB, *et al.* Multiphoton fluorescence excitation: New spectral windows for biological nonlinear microscopy. *Proc Natl Acad Sci USA* 1996;93:10763–10768.
29. Williams RM, Zipfel WR, Webb WW. Multiphoton microscopy in biological research. *Curr Opin Chem Biol* 2001;5:603–608.
30. Dunn KW, Sandoval RM, Kelly KJ, *et al.* Functional studies of the kidney of living animals using multicolor two-photon microscopy. *Am J Physiol Cell Physiol* 2002;283:C905–916.
31. Chaigneau E, Oheim M, Audinat E, *et al.* Two-photon imaging of capillary blood flow in olfactory bulb glomeruli. *Proc Natl Acad Sci USA* 2003;100:13081–13086.
32. Brown EB, Campbell RB, Tsuzuki Y, *et al.* In vivo measurement of gene expression, angiogenesis and physiological function in tumors using multiphoton laser scanning microscopy. *Nat Med* 2001;7:864–868.
33. Oheim M, Beaurepaire E, Chaigneau E, *et al.* Two-photon microscopy in brain tissue: Parameters influencing the imaging depth. *J Neurosci Methods* 2001;111:29–37.
34. Vérant P, Serduc R, Coles JA, *et al.* A method for measuring cerebral blood volume of mouse using multiphoton laser scanning microscopy. Proceedings of the International Society for Optical Engineering (SPIE), Femtosecond laser applications in biology. Vol. 5463. Strasbourg; 2004. p. 1–12.
35. Fuss M, Wenz F, Scholdei R, *et al.* Radiation-induced regional cerebral blood volume (rCBV) changes in normal brain and low-grade astrocytomas: Quantification and time and dose-dependent occurrence. *Int J Radiat Oncol Biol Phys* 2000;48:53–58.
36. Dilmanian FA, Kalef-Ezra J, Petersen MJ, *et al.* Could X-ray microbeams inhibit angioplasty-induced restenosis in the rat carotid artery? *Cardiovasc Radiat Med* 2003;4:139–145.
37. Reidy MA, Schwartz SM. Endothelial regeneration. III. Time course of intimal changes after small defined injury to rat aortic endothelium. *Lab Invest* 1981;44:301–308.
38. van Vulpel M, Kal HB, Taphoorn MJ, *et al.* Changes in blood-brain barrier permeability induced by radiotherapy: Implications for timing of chemotherapy [Review]? *Oncol Rep* 2002;9:683–688.
39. Dilmanian FA, Hainfeld JF, Kruse CA, *et al.* Biological mechanisms underlying the X-ray microbeam effects of preferentially destroying tumors. In: Corwin MA, Ehrlich SN, eds. *National Synchrotron Light Source activity report 2002*. 2003.
40. Siegbahn E, Brauer-Krisch E, Stepanek J, *et al.* Dosimetric studies of microbeam radiation therapy (MRT) with Monte Carlo simulations. *Nucl Instrum Methods Phys Res A: Accelerators, Spectrometers, Detectors and Associated Equipment* 2005;548:54–58.
41. Slatkin DN, Spanne P, Dilmanian FA, *et al.* Microbeam radiation therapy. *Med Phys* 1992;19:1395–1400.
42. Brauer-Krisch E, Bravin A, Lerch M, *et al.* MOSFET dosimetry for microbeam radiation therapy at the European Synchrotron Radiation Facility. *Med Phys* 2003;30:583–589.
43. Orion I, Rosenfeld AB, Dilmanian FA, *et al.* Monte Carlo simulation of dose distributions from a synchrotron-produced microplanar beam array using the EGS4 code system. *Phys Med Biol* 2000;45:2497–2508.
44. Slatkin DN. Uniaxial and biaxial irradiation protocols for microbeam radiation therapy. *Phys Med Biol* 2004;49:203–204.
45. Brauer-Krisch E, Requardt H, Regnard P, *et al.* New irradiation geometry for microbeam radiation therapy. *Phys Med Biol* 2005;50:3103–3111.
46. Stepanek J, Blattmann H, Laissue JA, *et al.* Physics study of microbeam radiation therapy with PSI-version of Monte Carlo code GEANT as a new computational tool. *Med Phys* 2000;27:1664–1675.